Journal of the Korean Nuclear Society
Volume 23, Number 1, March 1991

Comparison of the Cylindrical Geometry and the Planar Geometry for the Near-Field Radionuclides Transport Model

Chul-Hyung Kang, Kyong-Won Han, and Hun-Hwee Park
Korea Atomic Energy Research Institute

(Received October 8, 1990)

방사성 폐기물 처분장내 충전물질에서의 핵종 이동 모델의 원주좌표계와 평면좌표계에서 결과 비교

강철형 · 한경원 · 박헌휘
한국원자력연구소

(1990. 10. 8 접수)

Abstract

Many of the analyses of the transient radionuclide migration are approximated by an one-dimensional geometry and/or planar geometry. To validate these approximations, one should prove that these are reasonable and proper approximations. In this paper, the approximation which was in the study of the transport through backfill into a fissure is tried to validate. In that analysis, a cylindrical geometry was approximated by a planar geometry. The numerical illustrations show that the planar approximation agrees very well with the result of the cylindrical geometry for a ratio of the backfill outer radius to the waste form radius closed to unity. Even for a larger ratio of the two radii, the numerical difference is relatively small. Also the planar approximation which was used in the analysis gives conservative estimates.

요 약

처분장에서의 방사성 핵종 이동 연구에서 많은 학자들이 일차원 모델이나 평면좌표 모델을 가정하여 사용하고 있다. 이러한 시도들은 정당한 가정이라는 것을 보여야 할 것이다. 본 논문에서는 충전물질에서의 핵종이동에서 사용한 가정, 즉 원주좌표계를 평면좌표계로 단순화하였던 가정을 검증하고자 한다. 본 연구 결과, 충전물질층의 외경과 폐기물 고화체의 직경의 비가 1에 가까울수록 평면좌표계의 가정은 원주좌표계의 결과와 잘 일치함을 알 수 있으며 그 비가 커져도 두 좌표계의 오차는 상대적으로 적음을 알 수 있다. 또한 평면좌표계의 가정이 보수적인 결과를 준다.

1. Introduction

Fractures(fissures) in the emplacement rock of a geologic repository of nuclear waste may intersect boreholes for waste packages, providing conductive pathways for the hydrogeologic transport of radionuclides. This paper is concerned with the release of radionuclides from a waste form, surrounded by the backfill, which in turn is imbedded in a low porosity fissured rock formation. Fractures have permeabilities several orders of magnitude larger than the rock matrix itself. Thus water

flowing in the fissures provides a main hydrogeologic pathway for the transport of the nuclide into the far field region, see Figure 1. In that sense, one can assume the low porosity rock matrix surrounding the backfill is impervious to species transport. Therefore the nuclide released from a waste form diffuses through the water saturated backfill to a fissure intersecting the latter.

In previous study[1, 2], we assume a fixed concentration, i.e., solubility–limited concentration, at the surface of the waste form. The boundary condition at the backfill–fissure interface, i.e., "fissure opening" S_f (dotted area in Figure 1), is given by a mass balance of the diffusive flux from the backfill with the advective–diffusive transport of the species by the flowing water from the surface element S_f. The general form of this boundary condition is

$$-D_f \epsilon \nabla \hat{c} = \begin{cases} h(\hat{c}-\hat{c}_\infty), & \text{on } S_f \\ 0, & \text{on remainder of backfill-rock interface} \end{cases} \quad (1)$$

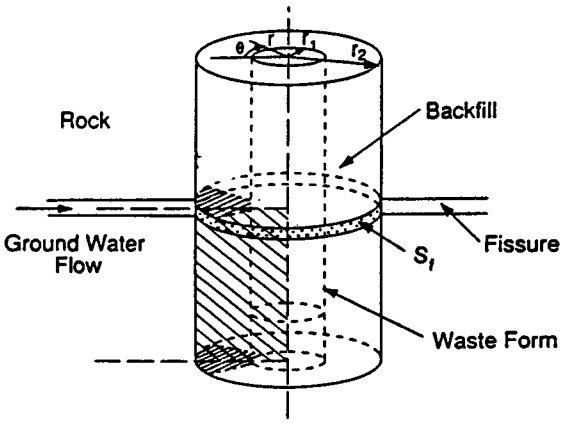

Figure 1. Schematic view of a bore hole intersected by a fissure in the nuclear waste repository.

where $\hat{c}$ is the species concentration on S_f, $\hat{c}_\infty$ is its concentration in the water far from the backfill, which without loss of generality will be taken equal to zero. h is the mass transfer coefficient, assumed constant over the entire surface S_f. D_f is the diffusion coeffcient of the species in the water saturated backfill, and ϵ the porosity of the backfill.

On account of the assumed independence of the boundary conditions with the cylindrical–polar coordinate angle θ, it suffices to analyze the problem in a sector of the canister and backfill, and one half of the fissure opening as shown in

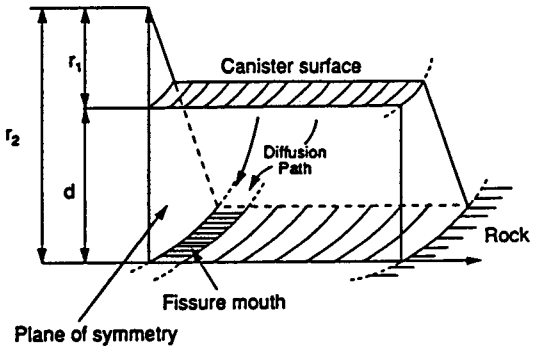

Figure 2. A sector of the backfill and one half of the fissure opening.

Figure 2. The latter produces a plane of symmetry on which the $\nabla \hat{c}=0$. This sector problem in turn can be simplified, if the ratio of the canister radius to backfill radius is of order unity. This implies a thin backfill region and the sector degenerates into a rectangular parallelopiped which can be described in a rectangular coordinate system. One of the coordinates, say z, is the replacement of the variable θ and thus need not be considered due to the assumed independence of the boundary conditions with θ. The resultant two–dimensional geometry is shown in Figure 3 with associated side conditions.

It is convenient to non–dimensionalize the species concentration $\hat{c}(x, y, t)$ with help of the species concentration $\hat{c}_s$ prescribed on the surface of the waste form ($0 \le x \le a$, $y=d$) and additionally set

$$c(x,y,t)=\frac{\hat{c}(x,y,t)}{\hat{c}_s}, \quad D=\frac{D_f}{K} \quad (2)$$

where K is the species' retardation coefficient in

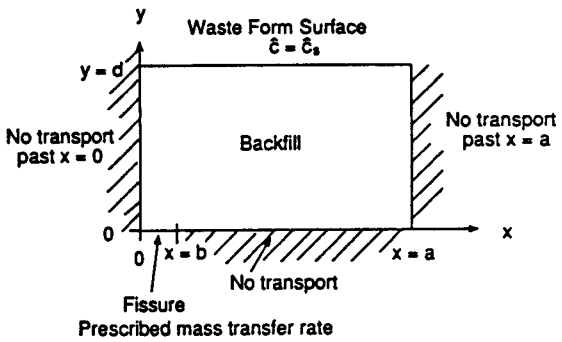

Figure 3. The planar geometry approximation.

the backfill.

The governing equation for $c=c(x, y, t)$ then reads

$$\frac{\partial c}{\partial t}=D\left(\frac{\partial^2 c}{\partial x^2}+\frac{\partial^2 c}{\partial y^2}\right)-\lambda c, \quad t>0,\ 0<x<a,\ 0<y<d,\ t>0 \tag{3}$$

with the side conditions

$$c(x,y,0)=0, \qquad 0<x<a,\ 0<y<d \tag{4}$$

$$\frac{\partial c(0,y,t}{\partial x}=\frac{\partial c(a,y,t)}{\partial x}=0, \quad 0<y<d,\ t>0 \tag{5}$$

$$c(x,d,t)=1, \qquad 0<x<a,\ t>0 \tag{6}$$

$$\frac{\partial c(x,0,t)}{\partial y}=\begin{cases}\dfrac{h}{D_f\epsilon}c(x,0,t), & 0<x<b\\ 0, & b<x<a\end{cases}, \quad t>0 \tag{7}$$

The boundary condition(7) is patterned after the equation(1). One should note that this problem is a mixed boundary condition problem on backfill/rock interface which is mathematically quite involved. In order to simplify the analysis, the spatial dependence of $c(x,0,t)$ on $0<x<b$ is replaced by an average concentration $[c(t)]_{av}$. Then the boundary condition can be written

$$\frac{\partial c(x,0,t)}{\partial y}=\begin{cases}\dfrac{h}{D_f\epsilon}[c(t)]_{av}, & 0<x<b\\ 0, & b<x<a\end{cases} \equiv \psi(x,t),\ t>0 \tag{7'}$$

where $[c(t)]_{av}$ is defined by

$$[c(t)]_{av}=\frac{1}{b}\int_0^b c(x,0,t)dx. \tag{8}$$

Note that, however, $[c(t)]_{av}$ is still an unknown function of time.

We now introduce the following dimensionless variables

$$X = x/a,\ Y = y/d$$

$$\tilde{\gamma}_i = \hat{\gamma}_i d,\ \tilde{\mu}_n = \mu_n a,\ \tilde{d} = d/a,\ \tilde{b} = b/a$$

$$\Lambda = \sqrt{\lambda d^2 K/D_f},\ \text{Modified Thiele modulus} \tag{9}$$

$$T = \frac{D_f t}{K d^2},\quad \text{Modified Fourier modulus}$$

$$Sh = \frac{hd}{D_f\epsilon},\quad \text{Modified sherwood modulus}$$

where

$$\hat{\gamma}_i=\frac{2i+1}{2}\frac{\pi}{d},\ i=0,1,\ \ldots$$

$$\mu_n=\frac{n\pi}{a},\ n=0,\ 1,\ \ldots \tag{10}$$

Then the solution can be written [2]

$$c(X,Y,T)=\frac{\cosh(\Lambda Y)}{\cosh(\Lambda)}+2\sum_{i=0}^{\infty}(-1)^{i+1}\frac{\tilde{\gamma}_i}{\tilde{\gamma}_i^2+\Lambda^2}e^{-(\tilde{\gamma}_i^2+\Lambda^2)T}\cos(\tilde{\gamma}_i Y)+$$

$$+2Sh\sum_{n=0}^{\infty}\delta_n\cos(\tilde{\mu}_n X)\frac{\sin(\tilde{\mu}_n\tilde{b})}{\tilde{\mu}_n}\sum_{i=0}^{\infty}(-1)^{i+1}\sin(\tilde{\gamma}_i[1-Y])\times$$

$$\times\int_0^T e^{-(\tilde{\gamma}_i^2+\tilde{\mu}_n^2\tilde{d}^2+\Lambda^2)(T-\tau)}[c(\tau)]_{av}d\tau,$$

$$0<X<1,\ 0<Y<1,\ T>0 \tag{11}$$

where

$$\delta_0=1\ ;\ \delta_n=2,\ n=1,\ 2,\ \ldots \tag{12}$$

Thus this solution is computed by solving a linear

Volterra integral equation.

The solution for cylindrical geometry can be derived with same procedures but contains one more variables, the inner radus. As one notice, this solution will be more complicated than the solution(12). Here we solve the early time solutions and steady state solutions for both geometries and compare with each others.

2. Early Time Solution for Cylindrical Geometry

The governing equations for $c=c(r,z,t)$ in cylindrical geometry is

$$\frac{\partial c}{\partial t} = D\left[\frac{\partial^2 c}{\partial r^2} + \frac{1}{r}\frac{\partial c}{\partial r} + \frac{\partial^2 c}{\partial z^2}\right] - \lambda c \ , \quad r_1 < r < r_2 \ , \quad 0 < z < a \ , \quad t > 0 \tag{13}$$

with the initial condition

$$c(r,z,0) = 0 \ , \quad r_1 < r < r_2 \ , \quad 0 < z < a \tag{14}$$

and boundary conditions

$$\frac{\partial c(r,0,t)}{\partial z} = \frac{\partial c(r,a,t)}{\partial z} = 0 \ , \quad r_1 < r < r_2 \ , \quad t > 0 \tag{15}$$

$$c(r_1,z,t) = 1 \ , \quad 0 < z < a \ , \quad t > 0 \tag{16}$$

$$\frac{\partial c(r_2,z,t)}{\partial r} = \begin{cases} -\frac{h}{D_f \epsilon}[c(t)]_{av} \ , & 0 < z < b \\ 0 \ , & b < z < a \end{cases} \equiv \psi(z,t) \ , \quad t > 0 \tag{17}$$

where

$$[c(t)]_{av} = \frac{1}{b}\int_0^b c(r_2,z,t)\,dz \ . \tag{18}$$

In early times, most nuclides which diffuse into the backfill are used to fill up the backfill, thus the outer boundary condition imposed by the presence of the fissure, does not affect the concentration profile. The early time behavior can be predicted by solving the problem with an outer boundary condition of zero flux. Thus the diffusion path of the nuclide follows the r direction and the concentration is independent of the z direction at early times.

The governing equation can be simplified as follows:

$$\frac{\partial c}{\partial t} = D\left[\frac{\partial^2 c}{\partial r^2} + \frac{1}{r}\frac{\partial c}{\partial r}\right] - \lambda c(r,t) \ , \quad r_1 < r < r_2 \ , \quad t > 0 \tag{19}$$

with the initial condition

$$c(r,0) = 0 \ , \quad r_1 < r < r_2 \tag{20}$$

and boundary conditions

$$c(r_1,t) = 1 \ , \quad t > 0 \tag{21}$$

$$\frac{\partial c(r_2,t)}{\partial r} = 0 \ , \quad t > 0 \ . \tag{22}$$

The early time solution [1] for cylindrical geometry is

$$c(r,t) = 1 + \sum_{n=1}^{\infty} A_n U_0(\beta_n r)\, e^{-(\lambda + D\beta_n^2)t} + \sum_{n=1}^{\infty} A_n U_0(\beta_n r)\, \frac{\lambda}{\lambda + D\beta_n^2}\left[1 - e^{-(\lambda + D\beta_n^2)t}\right] \ , \quad r_1 \le r \le r_2 \ , \quad t \ge 0 \tag{23}$$

where

$$A_n = -\pi \frac{J_1^2(\beta_n r_2)}{J_1^2(\beta_n r_2) - J_1^2(\beta_n r_1)} \quad (24)$$

$$U_0(\beta_n r) = Y_0(\beta_n r_1)J_0(\beta_n r) - J_0(\beta_n r_1)Y_0(\beta_n r) \quad (25)$$

and β_n is the *n–th* root of

$$Y_0(\beta_n r_1)J_1(\beta_n r_2) - J_0(\beta_n r_1)Y_1(\beta_n r_2) = 0 . \quad (26)$$

The solution of the early time solution for planar geometry can be easily find with similar procedures, and the solution is the form of the first two terms of the time dependent solution (12).

3. Steady State Solutions

3.1. Planar Geometry

The governing equation for $c=c(x,y)$ under steady state conditions reads,

$$D\left(\frac{\partial^2 c}{\partial x^2} + \frac{\partial^2 c}{\partial y^2}\right) - \lambda c = 0 , \quad 0 < x < a , \ 0 < y < d \quad (27)$$

with the boundary conditions

$$\frac{\partial c(0,y)}{\partial x} = \frac{\partial c(a,y)}{\partial x} = 0 , \quad 0 < y < d \quad (28)$$

$$c(x,d) = 1 , \quad 0 < x < a \quad (29)$$

$$\frac{\partial c(x,0)}{\partial y} = \begin{cases} \frac{h}{D_f \varepsilon}[c]_{av} , & 0 < x < b \\ 0 , & b < x < a \end{cases} \equiv \psi(x) \quad (30)$$

$$[c]_{av} = \frac{1}{b}\int_0^b c(x,0)\,dx . \quad (31)$$

The solution of this equation system yields,

$$c(x,y) = \frac{\cosh(\gamma_0 y)}{\cosh(\gamma_0 d)} + \sum_{n=0}^{\infty} \delta_n \frac{\sinh(\gamma_n[y-d])}{a\gamma_n \cosh(\gamma_n)} \cos(\mu_n x) \times \int_0^a \psi(x') \cos(\mu_n x')\,dx' , \quad 0 \le x \le a , \ 0 \le y \le d . \quad (32)$$

with

$$\mu_n = \frac{n\pi}{a} , \quad \gamma_n^2 - \mu_n^2 = \frac{\lambda}{D} , \quad n = 0, 1, \ldots . \quad (33)$$

Equation(32) can be expressed with the detailed form of the boundary condition function $\psi(x)$ defined in (30) and the dimensionless variables defined in equation(9) as follows

$$c(X,Y) = \frac{\cosh(\Lambda Y)}{\cosh(\Lambda)} - Sh[c]_{av} \sum_{n=0}^{\infty} \delta_n \cos(\tilde{\mu}_n X) \frac{\sin(\tilde{\mu}_n X)}{\tilde{\mu}_n \sqrt{(\tilde{\mu}_n \tilde{d})^2 \Lambda^2}} \times \frac{\sinh\left(\sqrt{(\tilde{\mu}_n \tilde{d})^2 + \Lambda^2}\,[1-Y]\right)}{\cosh\left(\sqrt{(\tilde{\mu}_n \tilde{d})^2 + \Lambda^2}\right)} , \quad 0 \le X \le 1 , \ 0 \le Y \le 1 . \quad (34)$$

This solution can be also derived form the time dependent solution(12) with some mathematical procedures.

3.2. Cylindrical Geometry

The steady state governing equation for $c=c(r,z)$ is

$$D\left(\frac{\partial^2 c}{\partial z^2}+\frac{\partial^2 c}{\partial r^2}+\frac{1}{r}\frac{\partial c}{\partial r}\right)-\lambda c=0\ ,$$

$$0<z<a\ ,\quad r_1<r<r_2 \tag{35}$$

with the boundary conditions

$$\frac{\partial c(r,0)}{\partial z}=\frac{\partial c(r,a)}{\partial z}=0\ ,$$

$$r_1<r<r_2 \tag{36}$$

$$c(r_1,z)=1\ ,\quad 0<z<a \tag{37}$$

$$\frac{\partial c(r_2,z)}{\partial r}=$$

$$=\begin{cases}-\frac{h}{D_f\epsilon}[c]_{av}, & 0<z<b\\ 0, & b<z<a\end{cases}\equiv\psi(z) \tag{38}$$

where

$$[c]_{av}=\frac{1}{b}\int_0^b c(r_2,z)dz\ . \tag{39}$$

The solution[1] of this equation system yields, after some minor simplifications, to

$$c(r,z)=\frac{1}{K_0(\sqrt{\lambda/D}r_1)}\left[K_0(\sqrt{\lambda/D}r)-K_1(\sqrt{\lambda/D}r_2)\frac{g(\sqrt{\lambda/D}r)}{g'(\sqrt{\lambda/D}r_2)}\right]-$$

$$-\frac{h[c]_{av}}{D_f\epsilon}\sum_{n=0}^{\infty}\delta_n\frac{\sin(\mu_n b)}{\mu_n a\sqrt{\mu_n^2+\lambda/D}}\frac{g(\sqrt{\mu_n^2+\lambda/D}r)}{g'(\sqrt{\mu_n^2+\lambda/D}r_2)}\cos(\mu_n z)\ ,$$

$$0\le z\le a\ ,\quad r_1\le r\le r_2 \tag{40}$$

where

$$g(kr)=I_0(kr)K_0(kr_1)-K_0(kr)I_0(kr_1) \tag{41}$$

$$g'(kr)=I_1(kr)K_0(kr_1)+K_1(kr)I_0(kr_1) \tag{42}$$

with

$$\mu_n=\frac{n\pi}{a}\ ,\quad \gamma_n^2-\mu_n^2=\frac{\lambda}{D}\ ,$$

$$n=0,1,\ldots. \tag{43}$$

4. Numericai Illustrations

Figures 4 through 6 show comparisons of the normalized concentrations of the cylindrical geometry and the planar geometry for different r_2/r_2 ratios and $Sh=1$ at early times. In each figure the solid lines represent the normalized concentration for the planar geometry versus time with y/d as a parameter, and the dashed lines represent the normalized concentration for the cylindrical geometry versus time with $(r_2-r)/(r_2-r_1)$ as a parameter. The same values of y/d and $(r_2-r)/(r_2-r_1)$, i.e., $y/d=(r_2-r)/(r_2-r_1)$ mean the corresponding locations in the two different geometries. For the ratio of r_2/r_1 close to 1, the results of these two geometries agree with each other at early times. However as the time increase and/or the ratio of r_2/r_1 increase, the difference in the normalized concentration for the two geometries increases. For the same r_2/r_1 ratio, the difference becomes small near the waste surface. Even

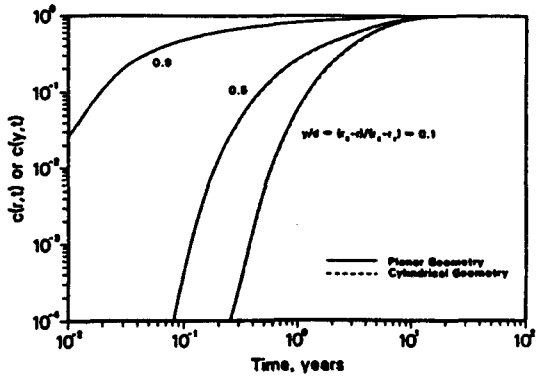

Figure 4. Comparison of the early time behavior of the cylindrical geometry and the planar geometry for r_2/r_1=1.1.

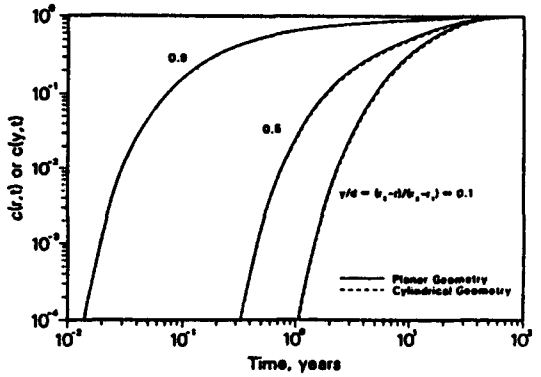

Figure 5. Comparison of the early time behavior of the cylindrical geometry and the planar geometry for r_2/r_1=1.2.

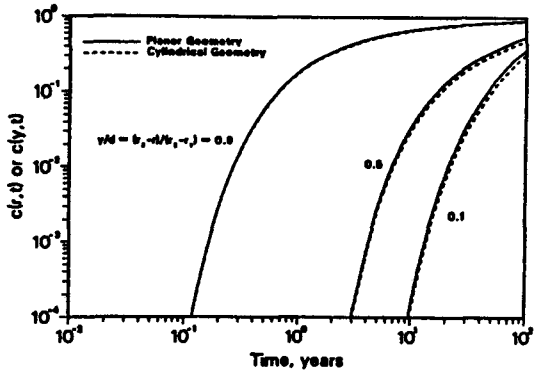

Figure 6. Comparison of the early time behavior of the cylindrical geometry and the planar geometry for r_2/r_1=1.6.

for a larger value of r_2/r_1 ratio, the difference is relatively small, see Figure 6. This ratio of r_2/r_1= 1.6 is close to a possible waste form–backfill design (e.g. 25cm waste canister radius and 15cm backfill layer).

Figures 7 to 9 show the comparison of the steady concentration profiles of the cylindrical geometry and the planar geometry for different r_2/r_1 ratios and for Sh= 1. In the figures solid lines represent the normalized concentration profile for planer geometry versus x/a with y/d as a parameter, and the dashed lines represent the

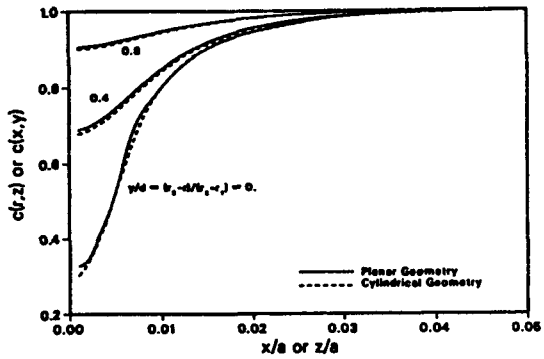

Figure 7. Comparison of the steady state concentration of the cylindrical geometry and the planar geometry for r_2/r_1=1.1 and Sh=1.

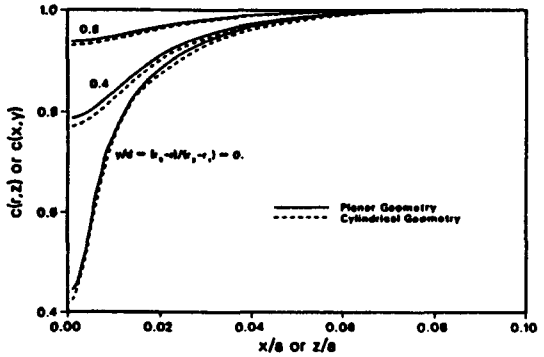

Figure 8. Comparison of the steady state concentration of the cylindrical geometry and the planar geometry for r_2/r_1=1.2 and Sh=1.

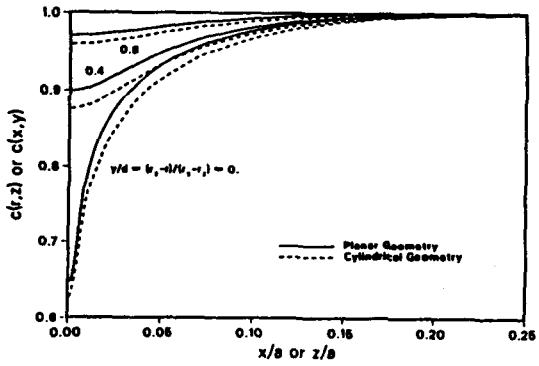

Figure 9. Comparison of the steady state concentration of the cylindrical geometry and the planar geometry for r_2/r_1=1.6 and Sh=1.

normalized concentration profiles for cylindrical geometry versus z/a with $(r_2-r)/(r_2-r_1)$ as a parameter. In the two geometries, the same values of $(x/a, y/d)$ and $(z/a, (r_2-r)/(r_2-r_1))$ represent the corresponding locations. As one expects, for a ratio of r_2/r_1 close to 1 the difference in the normalized concentration between two gometries is small, i.e., the planar geometry can be a good approximation of the cylindrical geometry. For the same r_2/r_1 ratio, the difference increases near the backfill and the fissure interface. Figure 9 shows the comparison of a r_2/r_1 ratio of 1.6, which is relatively large. The results from the two geometries differ, but the difference is less than 5%.

5. Conclusions

A cylindrical geometry is often approximated by a planar geometry in the study of the radionuclide transport through backfill into a fissure. In this paper, the planar approximation is tested and analyzed. The numerical illustrations show that the planar appro-ximation agrees very well with the result of the cylindrical geometry for a ratio of the backfill outer radius to the waste form radius close to unity. Even for a larger ratio of the two radii, the numerical difference is relatively small. Also the planar approximation which was used in the calculations[2] gives conservative estimates.

REFERENCES

1. Kang, C. H., *Mass Transfer and Transport of Radionuclides through Backfill in a Geologic Nuclear Waste Repository*, Ph. D. Dissertation, University of California, Berkeley(1989).
2. Kang, C. H. and P. L. Chambré, "The Radionuclide Transport through a Backfill Intersected by a Fissure," *Proc. KNS Autumn Annual Meeting*, 351(1989).